MATERIALS SELECTION FOR PRECISION INSTRUMENTS

D. Cebon and M.F. Ashby

Engineering Design Centre
University Engineering Department
Trumpington St, Cambridge, CB2 1PZ, UK

Meas. Science and Technology, Vol 5, pp296-306, 1994

ABSTRACT

This paper is concerned with the choice of the materials to minimise the deformation of mechanical components caused by extraneous thermal and vibrational inputs. First, material 'performance indices' (combinations of material properties) are derived for systems subjected to low frequency sinusoidal vibration inputs and for systems subjected to broad–band excitation. A methodology is developed for optimising the choice of material to minimise deformation due to vibration in such systems. Second, materials selection to minimise distortion caused by spurious thermal fluxes is discussed and a performance index which captures the relevant material property combinations is derived. Finally, a technique for reconciling the conflicting design goals of vibration and thermal distortion is considered.

The material selection procedure makes use of 'materials selection charts' - a new way of displaying material property data. When combined with the performance indices these allow a number of novel optimisation procedures. Section shape can be included, allowing the optimum selection of both material and shape. The method is illustrated through a case study involving selection of a material for the frame of an Atomic Force Microscope with sub–nanometre resolution.

1 INTRODUCTION

1.1 Design goals

Mechanical design often involves mechanical or thermal inputs which vary with time. Sometimes the goal is to minimise their influence: to evolve a design in which the response of the device to distortion caused by vibration or external heat fluxes is as small as possible. Sometimes the goal is the opposite: to maximise the response, or the speed of response. Often it is both: to maximise the response to one input but minimise that to others. An example is the design of mechanical transducers for precision instrumentation like atomic force microscopes. Here the design requirements are fast response-time and low susceptibility to disturbing signals. Similar requirements, though with differing emphasis, occur in the design of computer disk-drives, inertial guidance systems, mechanical testing equipment and even vehicle suspensions.

The requirement of minimising the vibration or thermal distortion of a critical component can be achieved either by isolating the component from the source of vibration or heat, or by designing the component and selecting its material so that it responds as little as possible to the inputs. The latter approach is the subject of this paper. A methodology is presented for selecting the best material for minimising the vibration of mechanical components and for minimising their distortion by thermal fluxes. The choice depends on the function and shape of the component and on the mode of loading. The methodology leads to a selection, from the full 'menu' of materials available to the engineer, of the material (or group of materials) with the optimum combination of properties to achieve one or the other of these goals. The materials chosen for minimum vibration and minimum thermal distortion are usually, different. General methods for reconciling these conflicting design goals are discussed in the last part of the paper.

1.2 Materials selection methodology

The method of selecting materials for each requirement has three ingredients. The first is the idea of a *materials-performance index (M)*: a combination of material properties which, if maximised, maximises one aspect of the performance of the component. A familiar example is the specific stiffness:

$$M_1 = E/\rho, \tag{1}$$

where E is Young's modulus and ρ is the density. Materials with large values of M_1 are good for light, stiff structures. In later sections of this paper performance indices for the design goals listed above will be developed. They involve various combinations of Young's modulus E, shear modulus G, density ρ, yield or fracture strength σ_f, loss coefficient η, thermal conductivity λ, and thermal expansion coefficient α.

The second ingredient in the selection methodology is the idea of a *materials-selection chart*. At its simplest, a materials-selection chart is a diagram with a pair of material properties as axes, for example E and ρ as shown in Figure 1. The scales are logarithmic and can, if desired, span a range so wide that all available materials can be included. When data for a given material class such as *metals* are plotted on these axes, it is found that they often occupy a characteristic field which can be enclosed in a 'balloon'. Ceramics also occupy a field, and so do polymers, elastomers, composites, and so on. The fields may overlap, but are nonetheless distinct. Individual materials or sub–classes (like steels in the metals field, or polypropylenes (PP) in that for polymers) appear as little 'bubbles' which define the ranges of their properties. All of the bubbles for one class of material are enclosed in a balloon: the metals–balloon, the polymers–

balloon, and so on. Almost always, further information can be plotted onto the chart. The longitudinal wave speed v_l (longitudinal speed of sound in the material) is plotted on Figure 1:

$$v_l = \sqrt{\frac{E}{\rho}}. \qquad (2)$$

Because of the logarithmic scales, contours of constant wave speed are a family of parallel lines of slope 1.

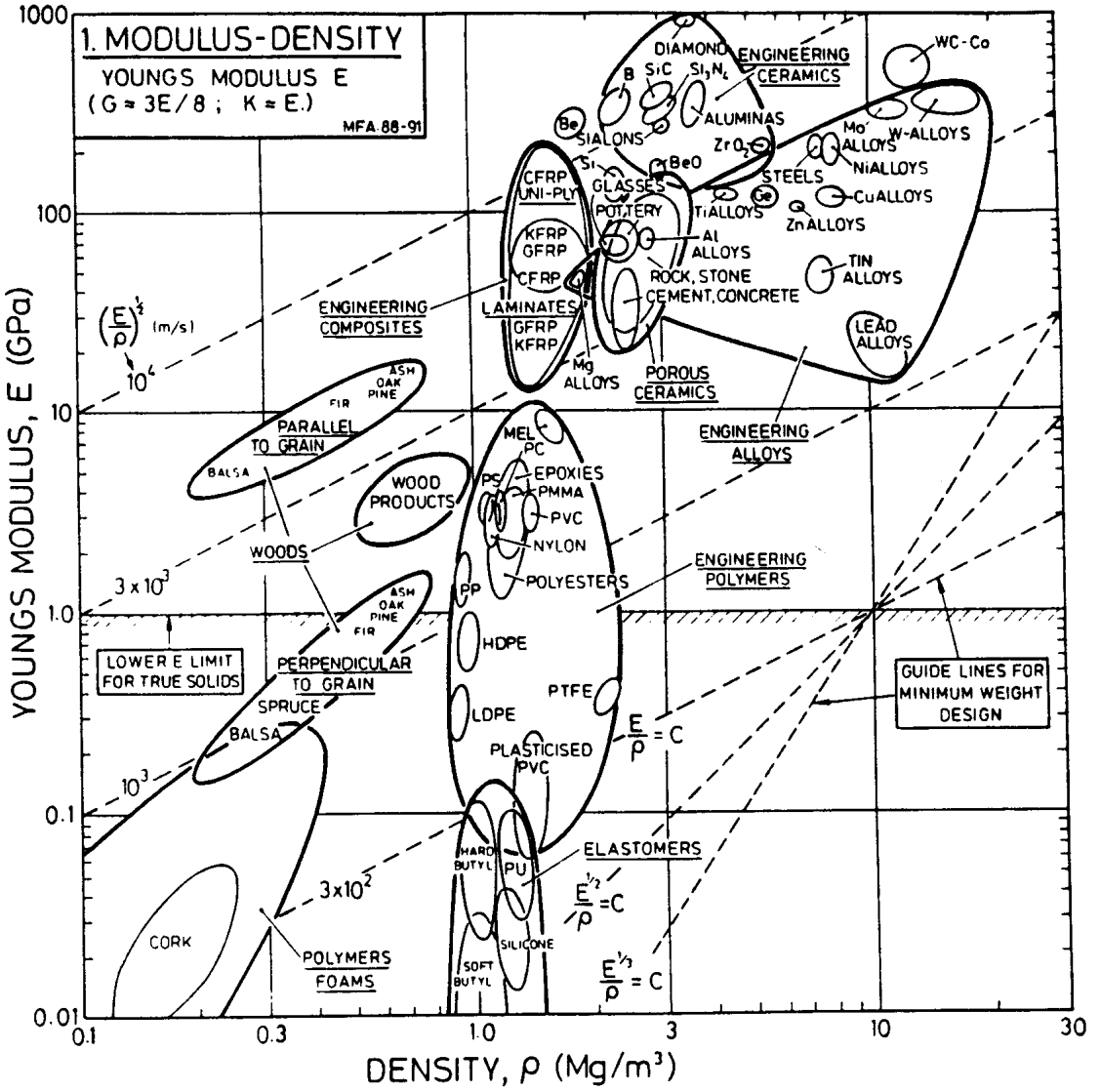

Fig. 1 A materials selection chart of Young's modulus E plotted against Density ρ. The logarithmic scales allow performance indices to be plotted as straight lines. The longitudinal wave speed $(E/\rho)^{1/2}$ appears as a set of diagonal contours.

Material selection charts can be used in conjunction with performance indices to optimise the choice of material. Consider the performance index M_1 defined by equation 1. Taking logarithms of both sides, it can be seen that contours of constant M_1 are lines of slope 1 on the chart - as were those for v_l. Materials with higher values of M_1 lie towards the top left corner of the chart. The grid of lines shows that these are ceramics like diamond (C) and silicon carbide (SiC), beryllium (Be) and Carbon Fibre Reinforced Plastic (CFRP). Figure 1 illustrates one of the simplest material selection charts. Many others are presented in [1]. Other charts can have combinations of materials properties as axes, and some of these are presented later.

The third ingredient in the selection methodology is that of characterising cross-sectional shape by a *shape factor* ϕ. Hollow tubular beams are lighter than solid ones for the same bending stiffness; box–section beams may be better still. The efficient shape gives extra stiffness for the same mass, as characterised by the second moment of area I. A convenient way to describe section-shape in stiffness-limited design is to define a dimensionless 'shape–factor', ϕ_B^e (B means 'bending', e means 'elastic') [2]:

$$\phi_B^e = \frac{4\pi I}{A^2}. \tag{3}$$

where A is the area of the cross–section. ϕ_B^e is dimensionless, and characterises the shape of the cross-section, independent of scale. The factor of 4π is included so that $\phi_B^e = 1$ for a solid circular section. Solid equiaxed sections (circles, squares, hexagons etc) all have values close to 1. Efficient shapes like thin–walled tubes or I–sections can have shape factors of 50 or more. The physical limit to ϕ_B^e is usually set by local buckling of the component. The maximum shape factor can be considered to be a material property and used profitably in the selection of materials. Other shape factors can be defined for design against yield or fracture (instead of stiffness) and for torsion as well as bending. Details of the methodology, with worked examples for static loading, can be found in [1, 2, 3].

1.3 Materials selection software

The procedure for materials selection, outlined above and detailed in the following sections has been implemented in a computer package called the Cambridge Materials Selector (*CMS*) which utilizes a database containing information about all classes of materials: metals, ceramics, glasses, polymers, composites and natural materials like wood. To select a material, the user performs a series of selection stages in which a pair of material properties of interest (or user-defined functions of material properties, like E/ρ) is specified. The program presents a graph or chart with these properties as the axes. All materials contained in the database with applicable data entries are plotted on each graph. The area of each graph which satisfies the selection criteria is specified by the user and the materials which lie in that area are considered to have 'passed' the selection stage. Up to six independent selection stages can be performed. The program stores the results of each selection stage and these can be examined at any time. *CMS* is described in [4]. Use of the software enables materials to be selected using complex charts which could not otherwise be plotted easily by hand. Materials selection charts generated by *CMS* are used to illustrate case studies later in this paper.

2 MATERIALS TO MINIMISE VIBRATION

Consider the problem of minimising the vibration of an item of very precise measuring or manufacturing equipment (a 'machine'), subject to vibration of its support. Accuracy problems are usually caused by *relative* dynamic deflection of some critical dimension of the machine, rather than *absolute* motion of the machine on its support. The design goal is, therefore, to minimise relative dynamic deflection of the machine. This can be achieved in two ways: (i) by isolating the machine from the excitation which causes it to vibrate [5], or (ii) by designing it to respond as little as possible to such inputs. Materials selection plays an important part in the second approach.

The analysis given below leads to two different types of performance index. The first applies when the lowest natural frequency of the system is much greater than that of the input. These indices generally involve the Young's modulus E the density ρ, and perhaps a shape factor ϕ. The second type of index applies when the excitation contains frequency components that coincide with natural frequencies of the system. Then the loss coefficient η (material damping) is important as well.

2.1 Performance indices for materials to resist sinusoidal inputs.

The first mode of vibration of such a machine can be modelled as a linear single degree–of–freedom oscillator with displacement input of its base x and relative displacement y, as shown in Figure 2a. (The machine may, in turn, be isolated from the vibrating input by a resilient isolator, but this does not affect the outcome of the following analysis.) Assume that the base of the machine vibrates at a single angular frequency ω, with input amplitude X, so that $x = Xe^{i\omega t}$. The relative deflection $y = Ye^{i\omega t}$ of a critical dimension of the machine is then given by the transfer function $H(i\omega)$:

$$H(i\omega) = \frac{Y}{X} = \frac{\left(\frac{\omega}{\omega_1}\right)^2}{1 - \left(\frac{\omega}{\omega_1}\right)^2 + i\,2\,\zeta_1\left(\frac{\omega}{\omega_1}\right)}, \tag{4}$$

where ω_1 is the undamped natural frequency and ζ_1 is the damping ratio.

The magnitude of $H(i\omega)$ is shown schematically in Figure 2b. It is apparent that minimum relative vibration is obtained at low excitation frequencies, since for small values of ω/ω_1,

$$|Y| \approx \left(\frac{\omega}{\omega_1}\right)^2 |X|, \qquad \frac{\omega}{\omega_1} << 1. \tag{5}$$

In order to minimise relative vibration of the machine for a sinusoidal input, it is therefore necessary to maximise the first natural frequency ω_1. Real machines, of course, have many modes of vibration, with complicated mode shapes, but the general conclusion of requiring maximum ω_1 is unaffected by this. Furthermore, the same conclusion is reached if it is assumed that the input to the system is an oscillating force applied to the mass, rather than a seismic displacement input applied to the base. Thus ω_1 is the quantity to be maximised: it is the *objective function*, in the language of optimisation theory.

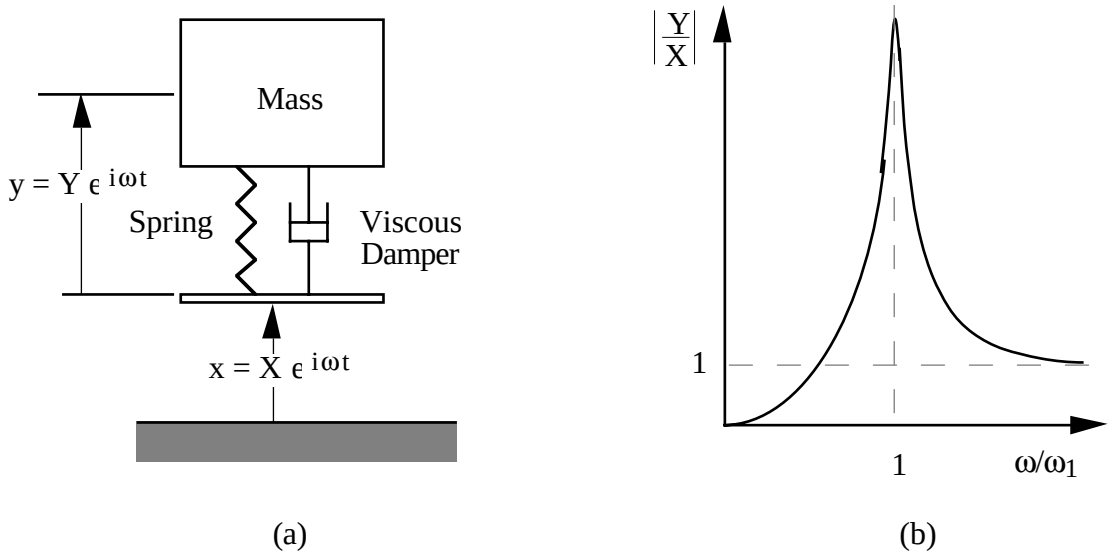

Fig. 2 (a) Single degree of freedom oscillator subject to displacement input x at frequency ω.
(b) Magnitude of the transfer function of the relative displacement y.

2.2 Example: performance index for undamped beam vibration

Consider, as an example, the derivation of a performance index for maximising ω_1 for a beam as shown in figure 3. Suppose that the beam is required to have a length L and a stiffness S, both specified by the functional requirements of the design, and it is to have the highest possible natural frequencies. The natural frequencies of flexural vibration of an Euler beam with cross–section area A, second moment of area I, Young's modulus E, and density ρ, are given by

$$\omega_n = a_n \sqrt{\frac{E\,I}{\rho\,A\,L^4}}, \qquad n = 1, 2, 3 \ldots \tag{6}$$

where n is the mode number and a_n is a constant that depends on the support conditions. For the simply supported beam shown in figure 3,

$$a_n = n^2\pi^2, \qquad n = 1, 2, 3 \ldots \tag{7}$$

Other support conditions change a_n, but not the other terms in equation 6.

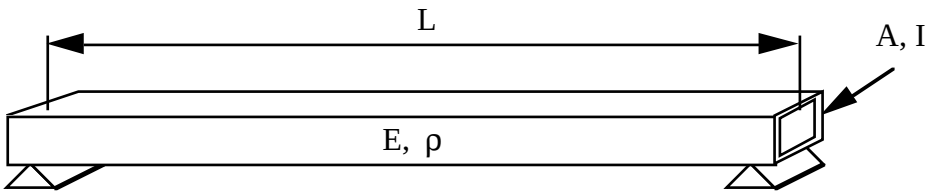

Fig. 3 Euler beam with length L, cross–section area A, second moment of area I, Young's modulus E and density ρ.

The stiffness of the beam is given by

$$S = \frac{C_1 E I}{L^3}, \tag{8}$$

where C_1 is a constant, like a_n, that depends only on the boundary conditions and loads. For the simply supported beam (carrying a central load) in figure 3, $C_1 = 48$. Other boundary conditions change C_1 but nothing else in equation 8.

The cross–section area A and the second moment of area I are 'free' variables: we wish to choose A and I so as to maximise the natural frequencies, while meeting the constraints imposed on L and S. Replacing A in equation 6 with the use of the shape factor in equation 3, and eliminating I with equation 8 gives:

$$\omega_n = \left[S^{1/4}\right] \left[\frac{a_n}{\left(4\pi\,L^5\,C_1\right)^{1/4}}\right] \left[\frac{\sqrt{E\phi_B^e}}{\rho}\right]^{1/2}. \tag{9}$$

The various terms have been grouped in brackets. The first bracket contains the *functional requirement* F and the second contains the *geometry* G, both of which are specified by the design. The third bracket contains the *material properties* M. (It is usual that the result of a modelling exercise to isolate a performance index can be separated is this way [6].) The flexural vibration frequencies of the beam can therefore be maximised by seeking the material with the largest value of

$$\left(\frac{\sqrt{E\phi_B^e}}{\rho}\right)^{1/2}. \quad \text{Hence the performance index is} \quad M_2 = \frac{\sqrt{E\phi_B^e}}{\rho}. \tag{10}$$

This selection is independent of the magnitude of the specified stiffness S, and of the length L, and of the details of the boundary conditions and loads contained in C_1 and a_n. The same material choice gives the maximum flexural vibration frequencies for *all* Euler beams.

Figure 4 shows a materials selection chart of $E\phi_B^e$ vs ρ generated by *CMS*. Each material is plotted as a bubble which represents the range of its two properties. A selection line has been drawn at $M_2 = 15.8\ GPa^{1/2}/(Mg/m^3)$. Unlike figure 1, this chart accounts for cross–section shape. As a result, light alloys such as those of aluminium and magnesium perform well because they can be manufactured with cross–sections that have large shape factors. The clear winner, however, is beryllium and its alloys, followed closely by unidirectional CFRP.

Balsa wood and foamed polymers could be used to make beams with high flexural vibration frequencies, but they may not be a suitable, because their cross sections A would have to be very large in order to provide sufficient stiffness. This can be shown by combining equations 3 and 8 to eliminate I, and solving for the 'free' variable A:

$$A = \left(\frac{4\pi L^3 S}{C_1}\right)\frac{1}{\phi_B^e E}\ . \qquad (11)$$

The term in brackets is fixed by the geometry and functional constraints. Therefore A is inversely proportional to $E\phi_B^e$. If the maximum acceptable value of A is limited by a space constraint ($A \le A_{lim}$), then this limiting value can be substituted into equation 11 and plotted as a horizontal line on the selection chart, as shown on figure 4. Beams made from materials lying below the horizontal line would have a value of A larger than the limiting size (in order to have a stiffness of S), and would therefore be unsuitable.

If it was not possible to manufacture the beam with a large value of the shape factor ϕ_B^e, then the best materials would be found by plotting a line of slope 2 on the E–ρ chart shown in figure 1. The best materials would then be ceramics such as diamond, silicon carbides, silicon nitrides, aluminas and pure silicon. Other possibilities are beryllium, or CFRP uniply. Aluminiums and magnesiums perform less well because they no longer have the advantage of the large shape factors.

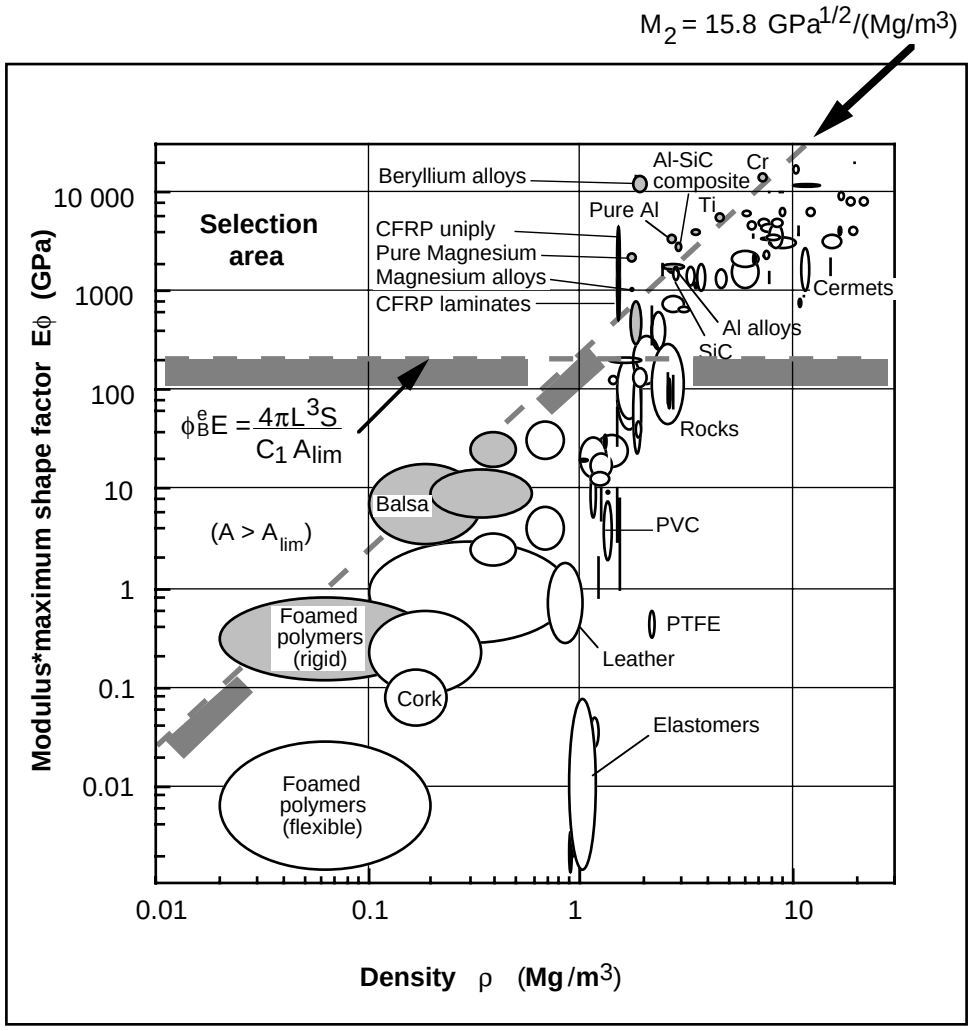

Fig. 4 Materials selection chart of $E\phi_B^e$ vs ρ generated by the Cambridge Materials Selector (*CMS*). Shaded materials are those that have 'passed' the selection stage. Beryllium alloys are the best choice for beams with high flexural vibration frequencies.

Table 1 contains performance indices M_u for maximising the lowest undamped vibration frequencies ω_1 of a variety of standard components: beams, plates, membranes etc. Most are functions of the Young's modulus E and density ρ, and sometimes a shape factor ϕ. When the price of the component is important, the cost per kg of the material C_R enters into the performance index. This accounts only for the cost of the raw material, and not the added cost of manufacture. For taut strings and membranes, the natural frequency depends on the applied tension, the maximum value of which depends on the failure strength σ_f of the material.

Component	*Specified*		
	Stiffness	*Mass*	*Cost*
Beam *Bending vibration.* Length fixed, section shape free.	$\left[\frac{\sqrt{E\,\phi_B^e}}{\rho}\right]^{1/2}$	$\frac{\sqrt{E\,\phi_B^e}}{\rho}$	$\left[\frac{E\,\phi_B^e}{\rho^2\,C_R}\right]^{1/2}$
Plate *Bending vibration.* Length & width specified, thickness free.	$\left[\frac{E^{1/3}}{\rho}\right]^{1/2}$	$\left[\frac{E}{\rho^3}\right]^{1/2}$	$\frac{E^{1/2}}{\rho^{3/2}\,C_R}$
Rod *Axial vibration.* Length specified, section area to be minimised.	$\left[\frac{E}{\rho}\right]^{1/2}$ and E	$\left[\frac{E}{\rho}\right]^{1/2}$ and $1/\rho$	$\left[\frac{E}{\rho}\right]^{1/2}$ and $1/\rho C_R$
Shaft *Torsional vibration.* Length specified, section area to be minimised.	$\left[\frac{G}{\rho}\right]^{1/2}$ and G	$\left[\frac{G}{\rho}\right]^{1/2}$ and $1/\rho$	$\left[\frac{G}{\rho}\right]^{1/2}$ and $1/\rho C_R$
Ring *Extensional vibration.* Radius specified, section area free to be minimised.	$\left[\frac{E}{\rho}\right]^{1/2}$ and E	$\left[\frac{E}{\rho}\right]^{1/2}$ and $1/\rho$	$\left[\frac{E}{\rho}\right]^{1/2}$ and $1/\rho C_R$
Ring *Bending vibration in or out of plane.* Radius specified, section shape free.	$\left[\frac{\sqrt{E\,\phi_B^e}}{\rho}\right]^{1/2}$	$\frac{\sqrt{E\,\phi_B^e}}{\rho}$	$\left[\frac{E\,\phi_B^e}{\rho^2\,C_R}\right]^{1/2}$
Ring *Torsional vibration.* Radius specified, section shape free.	$\left[\frac{E}{\rho}\frac{\phi_B^e}{\phi_T^e}\right]^{1/2}$ and E	$\left[\frac{E}{\rho}\frac{\phi_B^e}{\phi_T^e}\right]^{1/2}$ and $1/\rho$	$\left[\frac{E}{\rho}\frac{\phi_B^e}{\phi_T^e}\right]^{1/2}$ and $1/\rho C_R$
Taut string or membrane *Transverse vibration.* Length (width) specified, tension free.	$\left[\frac{\sigma_f}{\rho}\right]^{1/2}$ and E	$\left[\frac{\sigma_f}{\rho}\right]^{1/2}$ and $1/\rho$	$\left[\frac{\sigma_f}{\rho}\right]^{1/2}$ and $1/\rho C_R$

E = Young's modulus
ρ = Density
ϕ_B^e = Bending shape factor
σ_f = Failure strength.
G = Shear modulus
C_R = Cost per kg of raw material
ϕ_T^e = Torsion shape factor

Table 1 Performance indices M_u for maximising the lowest undamped vibration frequencies ω_1 of standard components, for specified stiffness, mass or cost.

Note that the performance indices in Table 1 are sometimes raised to a power (like the '1/2' in the first part of equation 10). Although these additional powers have no effect on selection charts like figure 4 (because they scale both axes of the selection chart equally), we will see later that they must be retained for material selections when the system is subject to broad–band excitation.

2.3 Material damping

All materials dissipate some energy during cyclic deformation, through intrinsic material damping and hysteresis. Damping becomes important when a component is subject to input excitation at or

near its resonant frequencies. This is the case when the excitation is 'broad–band' – that is, it covers a wide frequency range. Energy dissipation caused by friction in joints and air resistance are also important, but these are not considered here. This section discusses material damping. Material performance indices that incorporate damping are discussed in the next section.

There are several ways to characterise material damping. In this paper, we use the *loss coefficient* η which is a dimensionless number defined in terms of energy dissipation as follows. If a material is loaded elastically to a stress σ_{max} with corresponding strain ε_{max} (see figure 5) it stores elastic strain energy per unit volume u, where

$$u = \int_0^{\sigma_{max}} \sigma \, d\varepsilon = \frac{1}{2} E \varepsilon_{max}^2, \tag{12}$$

and E is the Young's modulus.

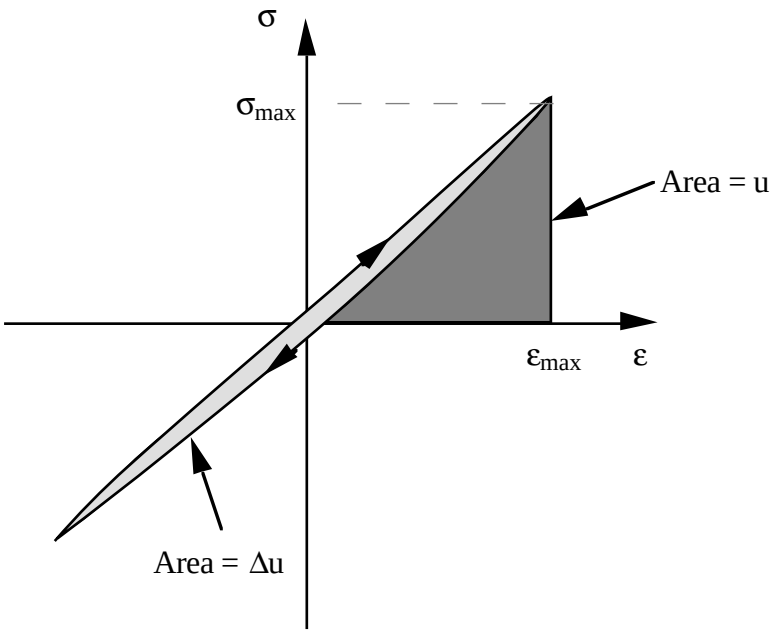

Fig. 5 Energy dissipated in a stress–strain cycle.

If the material is loaded and then unloaded, it dissipates energy equal to the area of the hysteresis loop shown in figure 5, given by

$$\Delta u = \oint \sigma \, d\varepsilon. \tag{13}$$

The loss coefficient η is the energy loss per radian divided by the maximum elastic strain energy (or the total vibrational energy):

$$\eta = \frac{\Delta u}{2\pi u}. \tag{14}$$

The value of η usually depends on the frequency of cycling, the temperature, and the amplitude of the applied stress or strain.

Other measures of damping include the proportional energy loss per cycle $D = \Delta u/u$, the damping ratio ζ, the logarithmic decrement δ, the loss angle ψ, and the quality factor Q [7]. When

damping is small ($\eta < 0.01$) and the system is excited near to resonance, these measures are related by [7]:

$$\eta = \frac{D}{2\pi} = 2\zeta = \frac{\delta}{\pi} = \tan\psi = \frac{1}{Q}. \tag{15}$$

They are not equivalent when damping is large.

Figure 6 is a material property chart of the loss coefficient η at 30 ˚C, plotted against the Young's modulus E. As a general rule, there is an inverse correlation between damping and modulus. Dense ceramics, and highly alloyed metals, have low damping because the dislocations they contain are strongly pinned. A few metals show anomalously high damping because of internal twinning (the Mn-Cu alloys, and perhaps magnesium). Other materials have high damping because they contain cracks which slide and dissipate energy due to friction (porous ceramics, cast irons). Polymers, when above their glass temperatures, show exceptionally high damping because molecular chains can slide; those below their glass temperature are still fairly lossy, because of the relative ease with which side-groups on the molecular chains can rearrange. This accounts for the obvious inverse dependence of η on E for polymers in figure 6. Indeed to a first approximation, $\eta = 0.1/E$, with E in GPa. (See Nashif et al [8] for further information about damping mechanisms.)

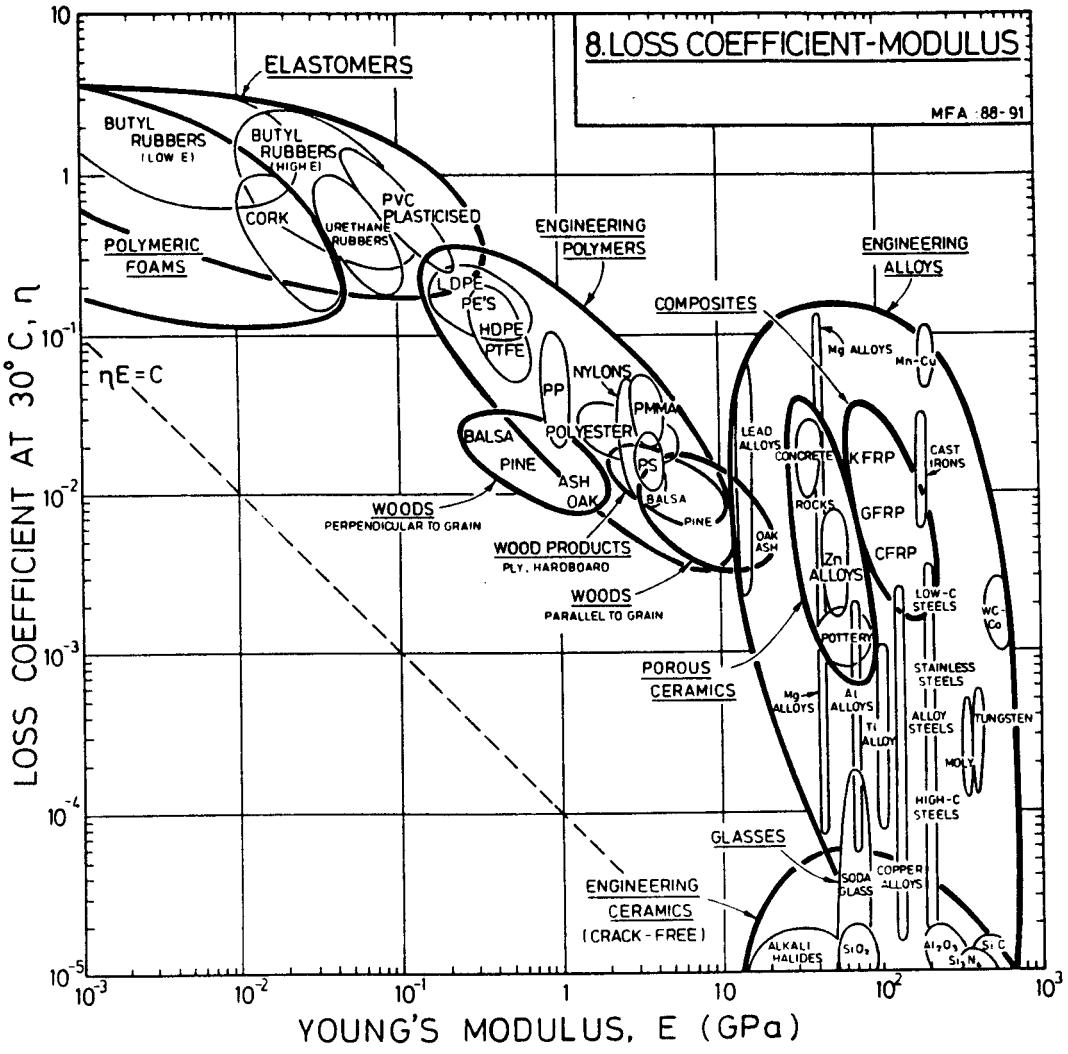

Fig. 6 Loss coefficient η plotted against Young's modulus E.

2.4 Performance indices for materials to resist broad band inputs

Now consider the vibration of a component that is excited over a wide frequency range, so that most of its response occurs around resonant frequencies, where damping is important.

Assume that the input x to the oscillator shown in figure 2a is stationary, random and broad–band, given by the generalised mean square ('power') spectral density $S_x(\omega)$, where

$$S_x(\omega) = S_0 \left(\frac{\omega}{\omega_0}\right)^{-k}. \tag{16}$$

S_0, ω_0 and k are constants, and k typically has a value greater than 2.

It is shown in the Appendix, that minimising the root mean square (RMS) deflection of the machine σ_y requires maximising the objective function

$$g(\omega_1, \zeta) = \zeta\, \omega_1^{k-1}. \tag{17}$$

where ω_1 is the first natural frequency of vibration, and ζ is the damping ratio which is assumed to be the same for all natural modes.

Now the loss coefficient and damping ratio are related by $\eta = 2\zeta$ (equation 15) and the first natural frequency ω_1 is proportional to the performance index for undamped vibration M_u, listed for various cases in Table 1. Thus the performance index for broad–band damped vibration is

$$M_d = \eta\, M_u^{k-1}. \tag{18}$$

The selection to maximise M_d can be performed by plotting a materials selection chart with $\log \eta$ on the x–axis and $\log M_u$ on the y–axis, and then plotting a selection line of slope $1/(1–k)$. The concept is shown schematically in Figure 7.

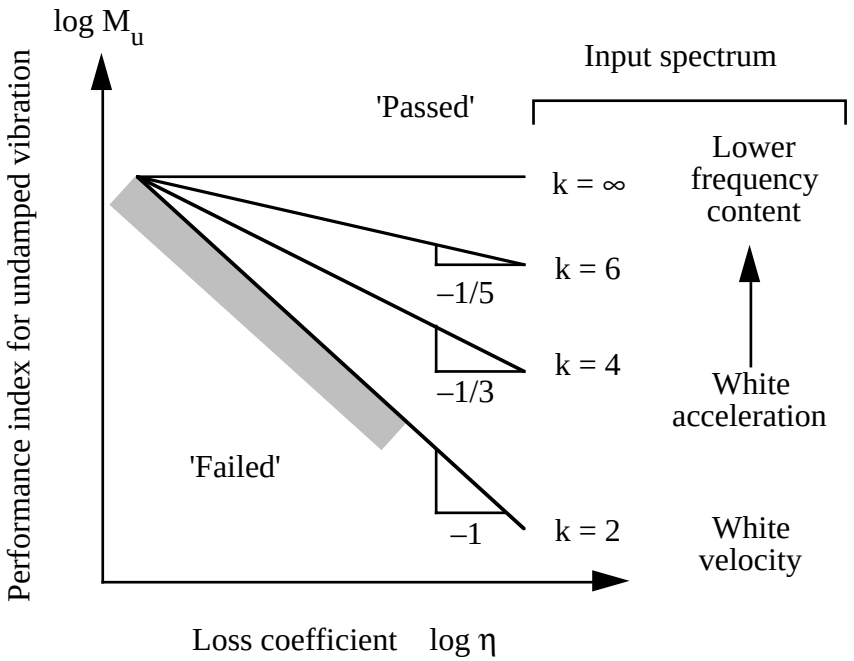

Fig. 7 Schematic diagram of a materials selection chart for minimising the RMS deflection of a component subject to an input with spectral density $S_0(\omega/\omega_0)^{-k}$. The performance index for undamped vibration M_u can be found in Table 1 for some standard cases.

If k = 0, the spectrum of input *displacement* is constant, corresponding to a 'white noise' input. This is generally not a practical case, because it implies infinite power input to the system. If k = 2, the spectrum of the input *velocity* is constant (or white), which just gives finite power. In this case the slope of the selection line (on the log–log plot) is –1. For k > 2, the input becomes more concentrated at low frequencies, and the selection line is less steep. When $k \rightarrow \infty$, the selection line becomes horizontal and the selection task becomes one of choosing materials with the highest value of M_u, exactly as for the undamped (sinusoidal input) case. Plotting the selection graph and performing the selection is difficult by hand, but straightforward using the *CMS* software described in section 1.3. A case study example follows.

2.5 Case study: materials for sub–nanometre displacement measuring devices

Figure 8 shows schematically, two precision measuring devices. The micrometer on the left illustrates the essential features of such a device: an actuator, a sensor, and a stiff force loop which supports the weight and provides a fixed reference. The Atomic Force Microscope (AFM) on the right has the same basic components (actuator, sensor, and force loop), however the sensor is a microscopic cantilever with an atomically sharp tip that is scanned across the surface of the sample. Deflection of the tip is measured by detecting the position of the reflected laser beam (sensor). A feedback control system maintains the deflection of the cantilever constant by moving the specimen up and down with a piezo–electric crystal (actuator). The signal controlling the crystal is therefore related to the profile of the surface. AFMs can achieve atomic resolution, better than 0.2nm [9].

We aim to choose materials for the frame (force loop) of the AFM. Strength is not a limiting factor, and the stiffness of the force loop is specified by functional constraints. The two important sources of error that we will consider in this paper are deflections of the force loop due to vibration and distortion caused by temperature fluctuations and thermal gradients.

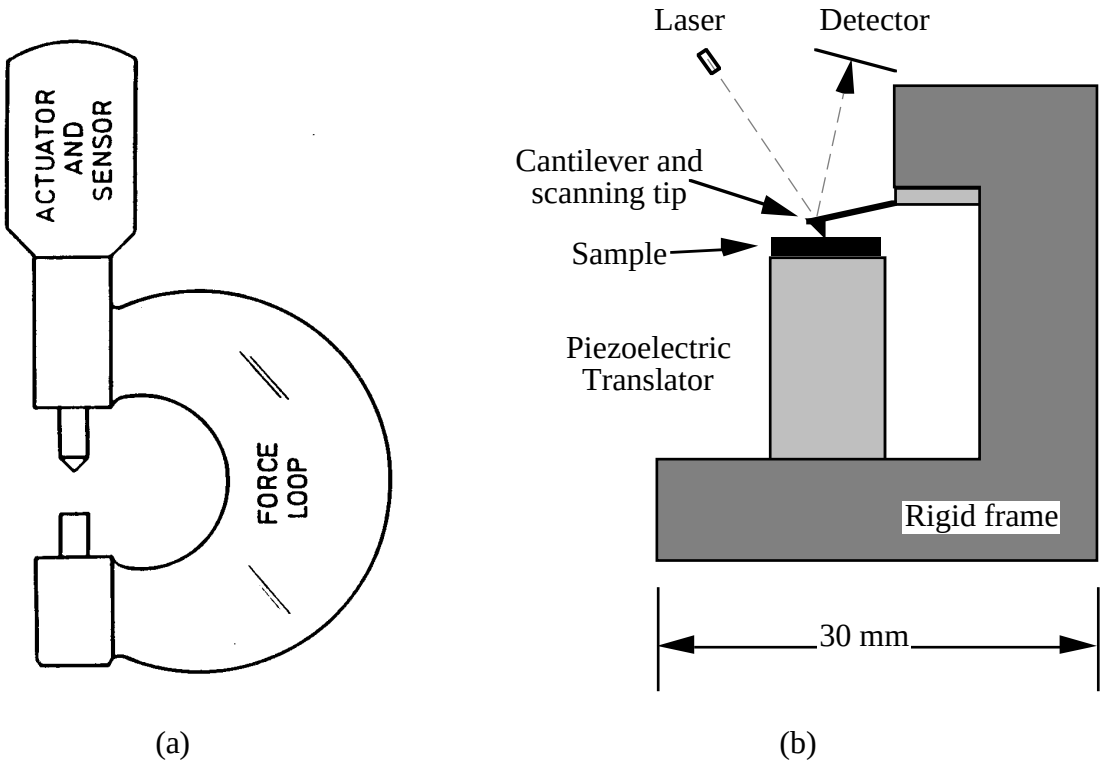

Fig. 8 A schematic diagram of two precision measuring devices.
(a) Micrometer (b) Atomic Force Microscope.

It is assumed that vibration of the force loop (frame) of the AFM is dominated by bending motion and that it can be modelled as an Euler beam (or as a combination of beams). In this case the performance index for undamped vibration is therefore $M_u = M_2^{1/2}$ as defined by equations 9 and 10. The power of 1/2 is retained because ω_1 is proportional to $M_2^{1/2}$ (see eq. 9 and Table 1).

The performance index for damped vibration of the AFM (from equation 18) is then:

$$M_3 = \eta\, M_u^{k-1} = \eta\, M_2^{(k-1)/2} = \eta \left[\frac{(E\phi_B^e)^{1/2}}{\rho} \right]^{(k-1)/2} . \qquad (19)$$

The spectral density of ambient vibration applied to the base of an AFM depends on many factors, in particular the sources of excitation (eg traffic on nearby roads, human movement and machinery in the building), vibration transmission paths through the building, and the foundation characteristics of the instrument. A reasonable assumption in the frequency range of interest (supported by measurements in the Cavendish Laboratory in Cambridge) is that the foundation vibrates with a 'white velocity' spectrum, (displacement proportional to ω^{-2}).

A precision instrument like an AFM is normally mounted on an isolation table with a soft suspension to isolate it from the ambient vibration. If the suspension is undamped and well designed, it (theoretically) behaves like a second order filter at high frequencies, in the range of vibration of the AFM frame. However, if any viscous damping is present in the suspension, to prevent large amplitude excursions (at low frequencies), the isolation table behaves like a first order filter at high frequencies. In this case the magnitude of the transfer function between foundation displacement and table displacement at high frequencies is $2\zeta_s\omega_s/\omega$, where ζ_s is the damping ratio of the isolation table and ω_s is its natural frequency. This is a more realistic case and will be assumed here.

The vibration spectrum input to the AFM at high frequencies can be calculated by combining the ground vibration input spectrum with the square of the transfer function of the isolation table, using random vibration theory (ie equation A1).

This gives:

$$S_x(\omega) = S_0 \left(\frac{\omega}{\omega_0} \right)^{-4} \qquad \omega >> \omega_s, \qquad (20)$$

where the value of $S_0\, \omega_0^4$ depends on the ground vibration input spectrum, and the damping ζ_s and natural frequency ω_s of the vibration isolation system. It is concluded that a suitable value for k in equation 16 is $k = 4$.

A materials selection chart of M_u vs η is shown in figure 9. The selection line has slope $1/(1-k) = -1/3$, as required by equation 18. Among the metals, magnesium and its alloys have the best performance because of their high internal damping and relatively high values of M_u. Although beryllium has a very high value of M_u it has low damping and therefore does not perform as well as magnesium. Cast irons (CI) perform approximately as well as berylliums, despite their low natural frequencies, because of their very high damping. Another possible choice is CFRP, although it may be difficult to form into an accurate shape in this application. Various polymers have good vibration performance, however they would require components with large cross sections to provide sufficient stiffness S (equation 11), and are therefore unsuitable. (The thermal properties of polymers are also unsuitable, as shown in the next section.)

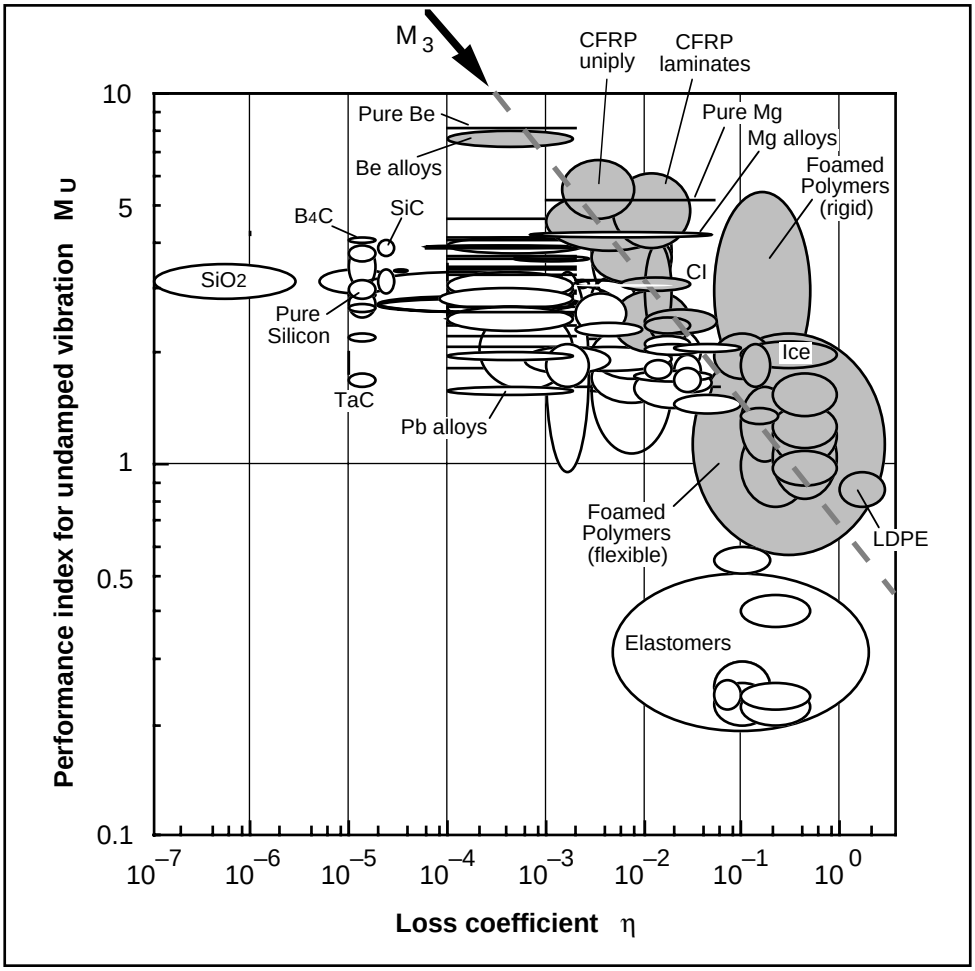

Fig. 9 Materials selection chart from *CMS* for damped vibration of the AFM frame. Among the metals, magnesium and its alloys are the clear winners.

3 MATERIALS TO MINIMISE THERMAL DISTORTION

Consider next a second source of inaccuracy: that caused by thermal distortion. In normal use, all mechanical devices encounter heat inputs caused by power dissipation in electronics, by human handling, thermal radiation and so on. Corrections to cope with thermal expansion are straightforward, provided the device is at a uniform temperature. *Thermal gradients* are the real problem: they cause a change of shape (distortion) of the device, for which compensation is not possible. Thus, in precision instrument design, it is permissible to allow expansion, provided distortion does not occur [10].

3.1 Performance indices for materials to resist thermal distortion

The essential ideas are captured by the following simple model. Consider a simply supported beam of length L and thickness h, one face of which is exposed to a fluctuating heat flux of intensity q (J/m^{2}s), see figure 10. The heat flux sets up a temperature gradient dT/dy, across the beam. If the period of the fluctuations in q is greater than the thermal response time of the beam $h^2/2a$ (where $a = \lambda/\rho C_p$ is the thermal diffusivity, λ the thermal conductivity, ρ the density and C_p is the specific heat capacity), then a steady state is reached with a temperature gradient given by Fourier's Law:

$$q = -\lambda \frac{dT}{dy}. \qquad (21)$$

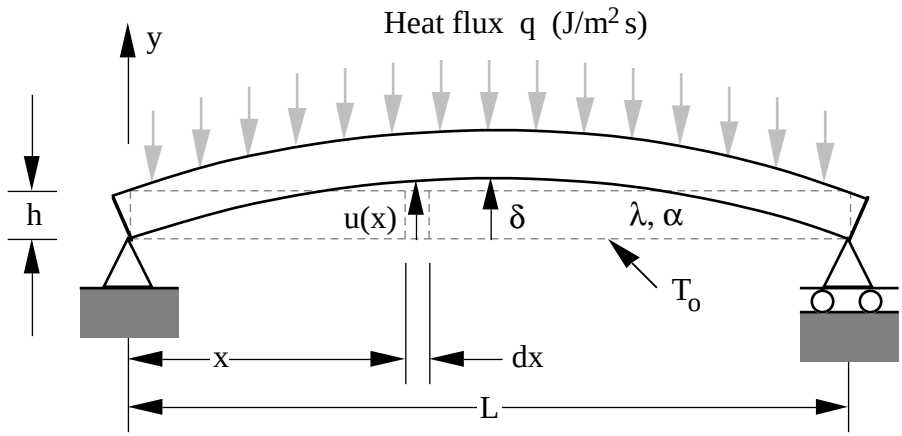

Fig. 10 A simply supported beam with a heat flux incident on one surface.

The thermal strain is related to temperature by

$$\varepsilon = \alpha\,(T_0 - T), \tag{22}$$

where α is the coefficient of thermal expansion and T_0 is the ambient temperature. A temperature gradient creates a strain-gradient $d\varepsilon/dy$ in the beam, causing it, if unconstrained, to take up a constant curvature K such that:

$$K = \frac{d^2u}{dx^2} = \frac{d\varepsilon}{dy} = \alpha\frac{dT}{dy} = \frac{\alpha}{\lambda}\,q, \tag{23}$$

where u is the transverse deflection of the beam. Integrating along the beam, accounting for the boundary conditions, gives the central deflection δ:

$$\delta = C_2\,L^2\,q\left(\frac{\alpha}{\lambda}\right), \tag{24}$$

where C_2 is a constant like C_1, which depends only on the thermal loads and boundary conditions. For the simply supported beam in figure 10, $C_2 = 1/8$. For a fluctuating heat source, with amplitude Δq:

$$\Delta\delta = C_2\,L^2\;\Delta q\;\left(\frac{\alpha}{\lambda}\right). \tag{25}$$

Thus for a given geometry and heat input, the distortion is minimised by selecting materials with large values of the performance index

$$M_4 = \frac{\lambda}{\alpha}. \tag{26}$$

Other geometries of heat flow and other beam boundary conditions change C_2, but the performance index M_4 remains the same.

3.2 Case study: materials for measuring devices

Figure 11 is a materials selection chart from *CMS* for selecting materials with high values of $M_4 = \lambda/\alpha$. It shows the thermal expansion coefficient α plotted against the thermal conductivity λ. The diagonal selection line has a slope of 1.0: it corresponds to the condition

$$M_4 = \frac{\lambda}{\alpha} = 10^7 \quad \text{W/m}.$$

Materials below this line have values of λ/α greater than 10^7. Among the metals, good choices are: aluminium alloys, tungsten alloys, beryllium alloys, silver alloys and copper alloys. Among the ceramics, silicon, silicon carbide, tungsten carbide and particularly graphite and diamond have very low thermal distortion.

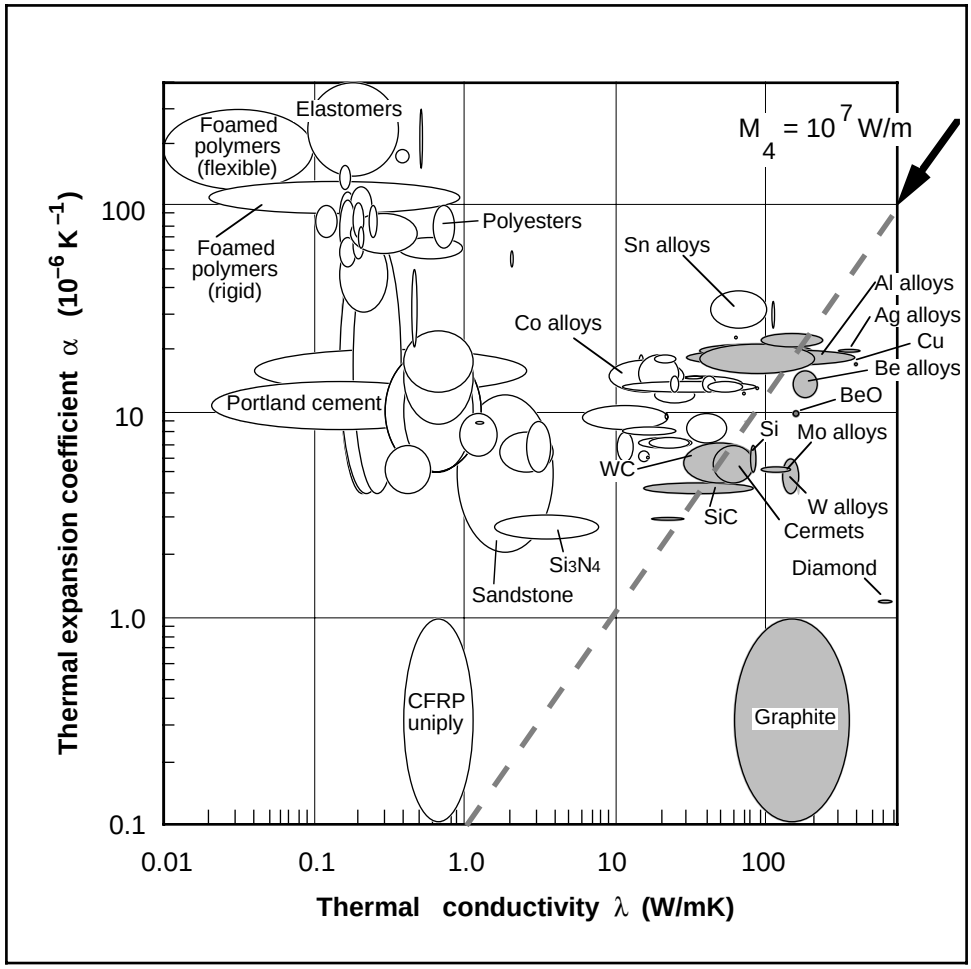

Fig. 11 The chart of thermal expansion against thermal conductivity, plotted by *CMS*, showing the selection of materials to minimise thermal distortion.

Suppose a precision instrument was required for applications in which the vibration input was below the first natural frequency of the structure, and that it was to be manufactured from solid sections with a low value of the shape factor ϕ_B^e. The best materials would then be those with high values of $E^{1/2}/\rho$ (found from figure 1) and λ/α (found from figure 11). Materials that perform best for both of these criteria are ceramics like pure silicon, silicon carbide (SiC) and diamond. Other possibilities are aluminium and beryllium alloys. In his analysis of this problem, Chetwynd [10] identified silicon as a good candidate material. It has a relatively high value of performance index M_4 and hence low thermal distortion. It is also relatively light and stiff and has high undamped natural frequencies. Furthermore it is available as large, pure, single crystals from which high quality components can be made.

4 CONFLICTING DESIGN GOALS

4.1 Methodology

Any real design imposes requirements which conflict. In the AFM example, the analyses above led to two different performance indices (M_3 and M_4) and two different sets of candidate-materials which minimise each sort of distortion separately. If the vibrational input was strong and the thermal one was weak, the designer might bias the choice towards members of the first set. If the opposite were true, then the bias might favour the second. This sort of problem is common in design, and is usually tackled by assigning arbitrary weighting factors which bias the choice towards the goal which, in the designer's view, is the more critical for overall performance. Such arbitrary decisions are a weakness because different designers will make different choices. The following method avoids them.

The key is to find a single measure – a common 'currency', so to speak – in which both design goals can be expressed. In many design problems the measure is simply that of cost. However, for critical components it is often *performance* and not cost that counts. Then a single measure of performance must be sought. We will illustrate the method by seeking the best material selection for the AFM frame, using, as a common measure, the distortion caused by imposed vibrational and thermal inputs.

4.2 Case study: materials for measuring devices

When the materials selection charts have logarithmic scales that span a wide range, it can be shown that the total distortion is least when the contributions from the two forms of deformation are equal. Equating the RMS vibrational distortion (equation A9) with the RMS thermal distortion* (equation 25) gives a *coupling equation* which links the two performance indices. For ω_1 from equation 9, with $a_1 = \pi^2$, $C_1 = 48$, and $C_2 = 1/8$, the result is:

$$M_3 = \left[\frac{25}{(L\,S^3)^{1/4}}\right]\left[\frac{S_0\,\omega_0^4}{(\Delta q)^2}\right] M_4^2. \qquad (27)$$

The first bracket contains functional constraints, which are prescribed by the design, and the second bracket contains a relationship between the two inputs Δq and $S_0\,\omega_0^4$. The best choice of material is now the one which maximises the two indices M_3 and M_4, and which also satisfies this equation. Thus it depends on the relative magnitudes of the two inputs.

Taking logs of equation 27 gives

$$\log_{10} M_3 = 2 \log_{10} M_4 + \log_{10}\left(\frac{25}{(L\,S^3)^{1/4}}\,\frac{S_0\,\omega_0^4}{(\Delta q)^2}\right). \qquad (28)$$

Figure 12 shows a materials selection chart generated by *CMS*, with M_4 plotted on the x-axis and M_3 on the y-axis. In order to choose the best material for a particular design, it is necessary to specify values for the input excitations Δq and $S_0\,\omega_0^4$, and for the beam length L and design stiffness S, and then to plot a line of slope 2 corresponding to equation 28 for these values. The set of parallel dashed lines on the chart correspond to equation 28, plotted for various values of the bracketted term. Two selection examples follow.

---

* A factor of $1/\sqrt{2}$ has been introduced to convert the amplitude of thermal distortion into an RMS value, assuming a sinusoidal input of amplitude Δq. A more accurate analysis could be performed if necessary, assuming a spectrum or Fourier series of thermal input.

If the thermal input Δq is large and the vibration input $S_0\,\omega_0^4$ is small, then equation 28 plots as a line towards the right of the chart, like line A–A. The best materials are then the ones furthest along this line, which fall into the box labelled *Selection 1*. These materials have high values of M_4 and intermediate values of M_3. Graphite, and tungsten (W) alloys have the best performance (approximately equal), and molybdenum (Mo) alloys also perform well.

Conversely if $S_0\,\omega_0^4$ is large and Δq is small, equation 28 plots as a line like B–B, nearer the left of the chart. The best materials are then the ones furthest along this line, which fall into the box labelled *Selection 2*. These materials have high values of M_3 and intermediate values of M_4. The best choice is clearly magnesium and its alloys, with CFRP uniply following close behind. Cast iron and beryllium alloys have approximately equal performance (although significantly different cost), and mild steel is also a reasonable choice.

Note that when the vibration input is considered to be broad–band, as in this example, pure silicon is no longer a good choice, because it has very low damping ($\eta \approx 10^{-5}$ in figure 9), and hence a low value of performance index M_3. It does not enter into either of the selection boxes shown in figure 12.

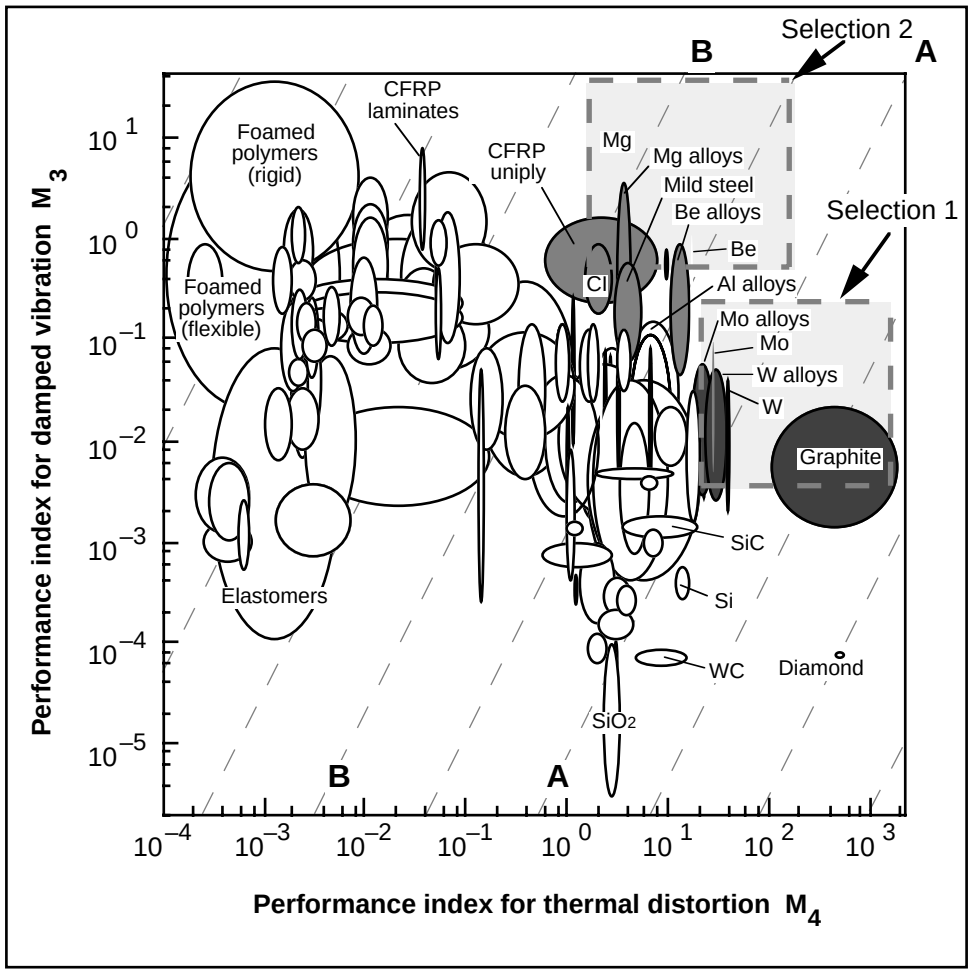

Fig. 12 Materials selection chart for the AFM, enabling a quantitative trade–off between vibration performance and thermal distortion.

5 CONCLUSIONS

A procedure with several novel features has been developed for selecting materials for components requiring low thermal distortion and low vibration.

(i) The procedure uses a novel display, the *Materials Selection Chart*, in conjunction with *Performance Indices* for selecting materials with optimum properties and shape. It has been implemented in an interactive computer program.

(ii) Performance indices have been developed for a number of standard design cases: for systems subjected to low frequency vibrational input and subject to broad–band vibration input; and for systems subject to thermal fluctuations. Vibrational distortion is minimised by maximising the lowest natural frequency of the component, or a combination of the lowest natural frequency and the loss coefficient. Thermal distortion is minimised by maximising a combination of thermal properties.

(iii) More sophisticated selections can be performed to trade–off apparently conflicting design goals, by expressing the selection criteria in terms of a common 'currency', in this case distortion of the instrument. Some surprising material choices result.

6 REFERENCES

1. Ashby MF, '*Materials selection in mechanical design*.' Pergamon Press, Oxford, 1992.
2. Ashby MF, 'Materials and shape.' *Acta Metall.*, 39 pp 1025–1039, 1991.
3. Ashby MF, 'On the engineering properties of materials.' *Acta Metall*, 37 pp 1273–1293, 1989.
4. Cebon D and Ashby MF, 'Computer–aided materials selection for mechanical design.' *Metals and Materials*, 8 (1) pp 25-30, 1992.
5. Harris CM and Crede CE, '*Shock and vibration handbook*.' McGraw Hill, 1976.
6. Cebon D and Ashby MF, 'Materials selection for mechanical design.' *Third international conference on the computerization and use of materials property data. Vol 3 of ASTM STP 1140, 1992.*
7. Newland DE, '*Mechanical vibration analysis and computation.*' Longman, Harlow, England, 1989.
8. Nashif AD, Jones DIG and Henderson JP, '*Vibration damping.*' Wiley Interscience, 1985.
9. Wong TMH and Welland ME, 'A digital control system for scanning tunnelling microscopy and atomic force microscopy.' *Meas. Sci. Technol.*, 4 pp 270–280, 1993.
10. Chetwynd DG, 'Selection of structural materials for precision devices.' Precision Engineering, 9 (1) pp 3–6, 1987.
11. Newland DE, '*Random vibrations and spectral analysis.*' Longman, 1984.

7 ACKNOWLEDGEMENTS

The authors are very grateful to the Leverhulme Trust for funding the initial development of the Cambridge Materials Selector, to Wei–Tatt Chong and Ruth Thomas for their programming, to Hugh Hunt for providing information about vibration levels in buildings, and to Mark Welland for useful discussions about atomic force microscopy.

APPENDIX: PERFORMANCE INDICES FOR BROAD–BAND VIBRATION

The spectral density $S_y(\omega)$ of the response of an oscillator to the ergodic random input $S_x(\omega)$ is given by the standard input/output relationship [11]:

$$S_y(\omega) = |H(\omega)|^2 S_x(\omega). \tag{A1}$$

The mean–square output σ_y^2 (square of the standard deviation) is found by integrating the output spectral density over all frequencies:

$$\sigma_y^2 = \int_0^\infty S_y(\omega)\ d\omega = \int_0^\infty |H(i\omega)|^2\, S_x(\omega)\ d\omega. \tag{A2}$$

The area under *each* resonant peak of the output spectrum $S_y(\omega)$ is approximately

$$\left(\begin{matrix}\text{Peak value}\\ \text{of } H(\omega_n)\end{matrix}\right)^2 \left(\begin{matrix}\text{Average value of } S_x(\omega)\\ \text{in the region of } \omega_n\end{matrix}\right) \left(\begin{matrix}\text{Mean square}\\ \text{bandwidth}\end{matrix}\right),$$

where the 'mean square bandwidth' is $\pi\zeta_n\omega_n$ [11]. Thus the integral can be approximated by a summation over all of the natural modes:

$$\sigma_y^2 \approx \sum_{n=1}^{\infty} |H(\omega_n)|^2\ S_x(\omega_n)\ \ \pi\zeta_n\omega_n. \tag{A3}$$

In order to perform this summation, it is helpful to make the following simplifications.

(i) When $\omega = \omega_1$, equation 4 gives $|H(\omega_1)| = 1/2\zeta_1$. It is straightforward to show that the same result holds for all natural modes in a multi–mode system. Therefore,

$$|H(\omega_n)| = \frac{1}{2\,\zeta_n}, \qquad n = 1, 2, 3, \ldots \tag{A4}$$

(ii) In the absence of detailed information about the variation of damping with frequency for all materials of interest, it is necessary to assume that all modes have the same damping ratio:

$$\zeta_n = \zeta, \quad \text{for all n.} \tag{A5}$$

This is a crude simplification. More accurate expressions could easily be included to account for the variation of damping with frequency, if such data was available.

(iii) For simple continuous systems, the frequencies of the second and higher natural modes of vibration can normally be written in terms of the first natural frequency ω_1. We introduce the function f(n), where

$$\omega_n = f(n)\ \omega_1. \tag{A6}$$

For example, for flexural vibration of beams, equations 6 and 7 give $f(n) = n^2$.

Substituting equations A4–A6 and 16 into equation A3 gives

$$\sigma_y^2 \approx \frac{\pi\, S_0\, \omega_0^k}{4} \left(\frac{1}{\zeta\, \omega_1^{k-1}}\right) \sum_{n=1}^{\infty} f(n)^{1-k} \tag{A7}$$

The mean square output σ_y^2 will be finite, providing the summation in equation A7 converges. The conditions for this convergence cannot be defined for the general case, however for the simply supported beam, for which $f(n) = n^2$, the summation will converge providing $2(1–k) < –1$, ie $k > 1.5$.† For axial or torsional vibration of rods with 'clamped-clamped' or 'free-free' end supports, or for transverse vibrations of strings; $f(n) = n$. In this case the convergence condition is $(1–k) < –1$, ie $k > 2$.

Providing the summation converges, the mean square displacement calculated from equation A7 is proportional to $1/\zeta\omega_1^{(k–1)}$. Therefore the root mean square (RMS) relative displacement σ_y, can be minimised by maximising the objective function

$$g(\omega_1, \zeta) = \zeta\omega_1^{k–1}. \tag{A8}$$

The AFM is assumed to be a beam with $f(n) = n^2$, subject to an input spectrum with $k = 4$. The summation in equation A7 is then close to 1.0, and equation A7 becomes:

$$\sigma_y \approx \left[\frac{\pi S_0\, \omega_0^4}{4\zeta\, \omega_1^3}\right]^{1/2}. \tag{A9}$$

† Note that for broad–band seismic input, the average kinetic energy of the foundation is proportional to the mean–square velocity. For this energy to be finite, it is necessary for k to be in the range $k \geq 2$.